Earthquakes and Structures, *Vol. 14, No. 5 (2018) 449-458*
DOI: https://doi.org/10.12989/eas.2018.14.5.449

Seismic performance of retrofitted URM walls with diagonal and vertical steel strips

Abbas Darbhanzi*[1], Mohammad S. Marefat[2a], Mohammad Khanmohammadi[2b], Amin Moradimanesh[2c] and Hamid Zare[2c]

[1]*College of Engineering, Vali-e-Asr University of Rafsanjan, Iran*
[2]*School of Civil Engineering, College of Engineering, University of Tehran, Iran*

(Received May 20, 2017, Revised March 18, 2018, Accepted March 19, 2018)

Abstract. Earthquakes have shown the vulnerability of unreinforced masonry (URM) structures. The aim of this research is to study a technique for in-plane seismic retrofitting of URM walls in which both diagonal and vertical steel strips are added to a single side of a URM wall. Specimens have been tested under quasi-static cyclic lateral load in combination with constant vertical load. The tests show that vertical and diagonal strips cause a significant increase in seismic capacity in terms of both strength (about 200%) and displacement at maximum (about 20%). Furthermore, this technique caused the failure modes of URM walls were influenced.

Keywords: seismic retrofit; clay brick; URM walls; vertical and diagonal steel strips; lateral strength and ductility

1. Introduction

It is known that the existing URM buildings are prone to earthquake forces and retrofitting of such buildings is an important concern worldwide (Abdul Karim *et al*. 2016, Remki *et al*. 2016, Preciado *et al*. 2015, Benedetti *et al*. 2014, Darbhanzi *et al*. 2014, Zuccarello *et al*. 2009). Various methods have been investigated for seismic retrofitting of URM walls such as confinement with reinforced concrete elements, adding fiber reinforced polymer (FRP) layers, reinforced concrete (RC) layers and post-tensioning. Popa *et al.* (2016), Wang *et al*. (2014), Mahmood *et al*. (2011) and Elgawady *et al*. (2006) have shown that retrofitting masonry walls with FRP sheets significantly increase their strength. Tena-Colunga *et al*. (2009) and Medeiros *et al*. (2013) have conducted a series of tests on masonry walls with horizontal and vertical reinforced concrete elements. They found that this technique causes significant improvement in both strength and ductility of URM walls and showed satisfactory performance against earthquakes. Ahmad *et al*. (2015) and Churilov *et al*. (2013) studied the effectiveness of two RC layer on URM walls. The results showed improvement in shear resistance of the retrofitted specimens. Mahjoob Farshchi *et al*. (2009) investigated the effect of post-tensioning on masonry walls and found that the technique increased in-plane lateral strength.

A technique of retrofitting URM walls using steel strips has been developed. This technique consists of adding diagonal and/or vertical steel strips on either one side or both sides of URM walls. Taghdi *et al*. (2000) and Farooq *et al*. (2012) carried out an experimental investigation on masonry walls with this method. The tests showed an increase in strength, ductility, and energy dissipation capacity. Darbhanzi *et al*. (2014) studied the effectiveness of vertical steel strips on URM walls. Four walls were tested under quasi-static cyclic lateral load in combination with constant vertical load: two specimens with steel strips and two without steel strips. These studies indicated that this technique causes significant improvement in both strength and ductility of URM walls and showed satisfactory performance against earthquakes.

Due to architectural considerations and neighborhood restrictions, it may not be possible to retrofit both sides of a wall. So, the aim of this research is to study a technique in which both diagonal and vertical steel strips are added to a single side of URM walls. In total, four half-scale specimens have been tested under quasi-static cyclic lateral load in combination with constant vertical load: two specimens without strips as reference specimens, two with steel strips fixed to foundation. This method has several advantages when compared to other methods such as simplicity to apply, relatively low costs, and insignificant disruption of service functions during repair.

2. Experimental program

The experimental research has been carried out in the structural laboratory of the University of Tehran. Details of the tests are described below.

∗Corresponding author, Ph.D.
E-mail: darbhanzi@vru.ac.ir
[a]Professor
E-mail: mmarefat@ut.ac.ir
[b]Associate Professor
E-mail: mkhan@ut.ac.ir
[c]MSc.

ISSN: 2092-7614 (Print), 2092-7622 (Online)

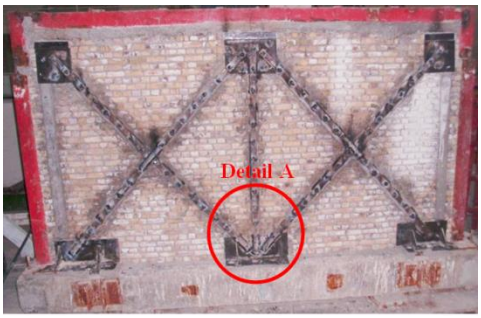

Specimen EMW11SR-3

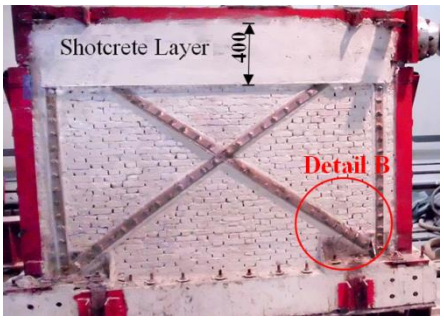

Specimen EMW21SSR-4

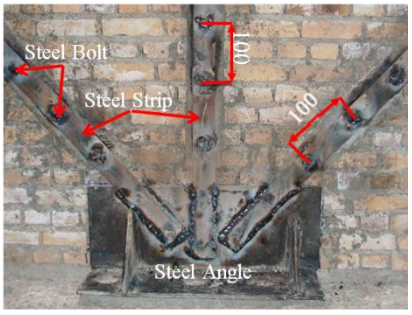

Detail A

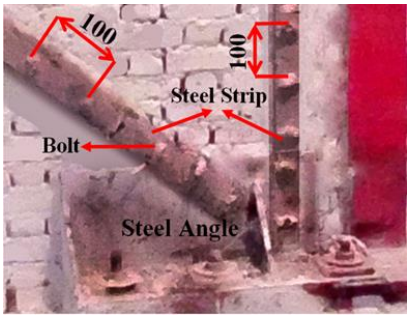

Detail B

Fig. 1 Details of retrofitting technique of specimens

110 mm thickness 160 mm thickness

Fig. 2 Masonry bond pattern

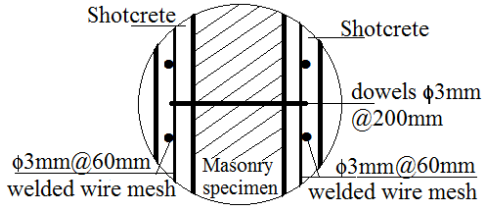

Fig. 3 Detail of Shotcrete on both sides

2.1 Test specimens

Specimens were built with two nominal dimensions of 1900×1400×110 mm (length×height×thickness) and 2700×1400×160 mm (length×height×thickness) in such way that represents real conditions of existing masonry buildings in Iran (sliding and diagonal tension failure modes). Specimens were retrofitted with vertical and diagonal steel strips (See Figs. 1-3 and Table 1). In the present research, the steel strips are externally applied to one face of the wall. The dimensions of steel strips were 30×3 mm (width×thickness).

For Specimen EMW11SR-3, first, 6 mm diameter holes were drilled at specified spacing (100 mm) in the masonry walls and in the steel strips. The spacing between these holes and thickness of steel strips are such that prevent buckling of the steel strips. Second, the steel bolts (5 mm diameter) were inserted into the drilled holes with epoxy resin and the steel strips were anchored to the masonry wall from one side. Third, the steel strips were welded to steel bolts and steel angles anchored into the concrete footing using 20 mm diameter anchor bolts, see Fig. 1.

For specimen EMW21SSR-4, first, steel strips anchored to the masonry wall from one side such as Specimen EMW11SR-3. Second, one layer of steel mesh of bar diameter of 3 mm and spacing of 60 mm was fixed by shear

Table 1 Specifications of different specimens

Specimen	Reference specimen	Specimen dimensions (mm)			Height to length ratio	Vertical loads (kN)
		Length	Height	Width		
URMW-1	-	2700	1400	160	0.5	43.2
URMW-2	-	1900	1400	110	0.7	20.9
EMW11SR-3	URMW-1	2700	1400	160	0.5	43.2
EMW21SSR-4	URMW-2	1900	1400	110	0.7	20.9

dowels (diameter of 3 mm at a distance of 200 mm) to top of both sides of the specimen (Fig. 3). The thickness of shotcrete layer was 12 mm. The shotcrete layer was added to support exiting steel plates and prevent their separation from the wall. The steel strips were protected by anti-oxide colours. The reference specimens of URMW-1 and URMW-2 had been previously tested (Darbhanzi *et al.* 2014).

All specimens were half scale in dimension with aspect ratios of 0.5 and 0.7 (height to length) and were tested under simultaneous static cyclic in-plane lateral load and constant vertical load. The specimens were constructed with solid clay bricks (105×49×31 mm) and cement mortar joints. The thickness of mortar joints was approximately 6 mm.

Table 2 Test results of materials

Material	Property	N	Mean (MPa)	SD (MPa)
Solid clay brick	compressive strength	9	8.7	1.90
Masonry	compressive strength	6	3.0	0.80
	Mortar joint shear strength	2	0.2	0.03
Steel strip	Yield tensile strength	3	280.3	2.50
	Ultimate tensile strength	3	363.9	8.30

Note: N: number of specimens; SD: standard deviation

2.2 Material properties

Characteristics of solid clay brick and mortar materials were approximately similar to those of existing URM buildings in Iran. Compressive strength tests of solid clay bricks and masonry prisms were carried out according to ASTM C67 (2002) and ASTM C1314 (2002), respectively. The mortar mixture contained one part cement, six parts sand and one part water (in volume) according to common construction practice in Iran. The water content of the mortar was adjusted to achieve a workable material according to local practices. In situ tests were carried out for shear strength of masonry mortar according to ASTM C1531 (2002). Tension tests were performed on samples of steel strips according to ASTM E8/E8M (2009). The results of tests are presented in Table 2.

2.3 Test setup

The experimental setup and views of the specimens are shown in Fig. 4. The specimens were constructed on a pre-cast reinforced concrete footing, which were anchored to the strong laboratory floor by means of steel rods, in order to prevent any vertical and horizontal movements. Lateral load was applied by a horizontal hydraulic jack with a maximum force capacity of 250 kN and a stroke of ±125 mm, which was connected to the horizontal steel beam on the top of the specimen and to the reaction steel frame. Lateral loads were measured by the load cell and recorded by a data logger.

Vertical load was also applied to the top of the specimen by means of a vertical hydraulic jack and using a rigid steel cross beam and anchor steel rod, as shown in Fig. 4. The value of the vertical loads includes the weight of the top steel cross beam plus the axial load of the vertical hydraulic jack, and these total values for all specimens are presented in Table 1. A set of Elastomeric bearings was placed between the steel beam on the top of specimens and the steel cross beam, in order to allow horizontal displacements of the specimens. Vertical load was applied in force control mode and was measured by a load cell built in the vertical hydraulic jack. The specimens were braced laterally to prevent out-of-plane movement.

2.4 Load patterns

A constant vertical axial compressive stress of 0.1 MPa was applied, in force control mode, to different specimens. Vertical load was uniformly distributed on the top of the specimens by means of rigid steel cross beam as shown in Fig. 4 and it was kept constant throughout the test. The distribution of the vertical load along the length of the specimens was not measured. The magnitude of vertical loads is shown in Table 1.

In-plane lateral load was applied to the specimens in

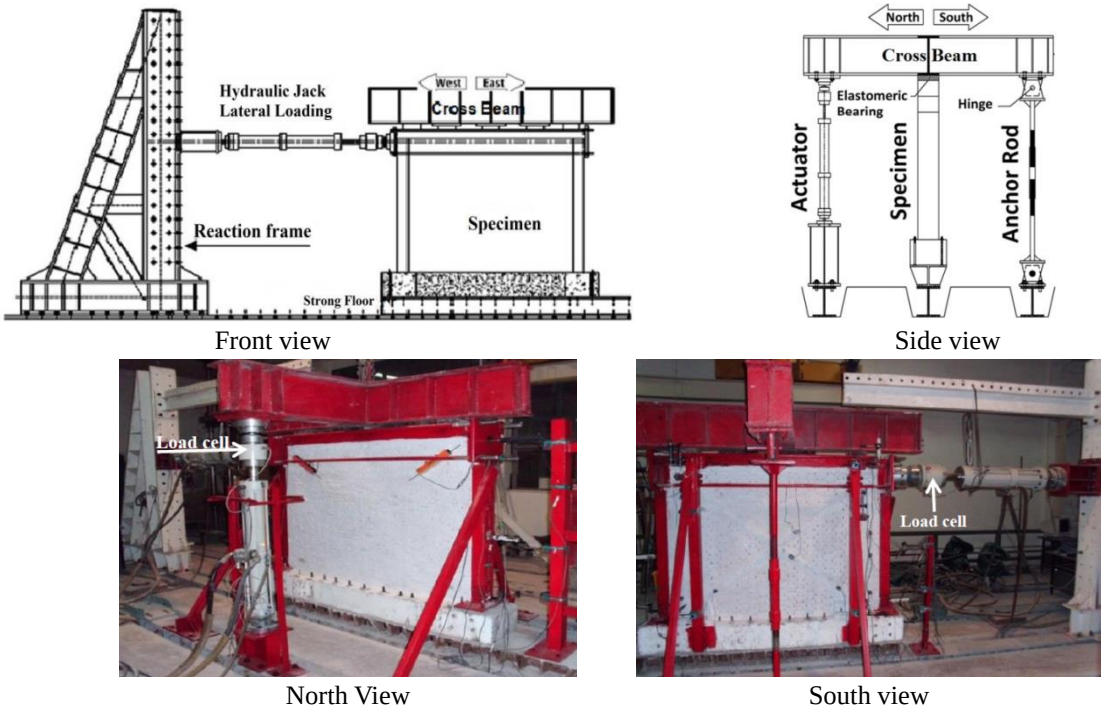

Front view Side view

North View South view

Fig. 4 Test setup

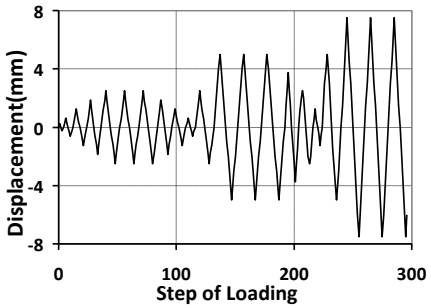

Fig. 5 Cyclic loading protocol

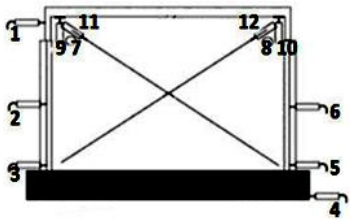

Fig. 6 Typical LVDTs arrangement

displacement control mode. For all specimens a cyclic displacement history as per TCCMAR sequential phased displacement recommendations was imposed (Porter, 1987). The cyclic load was applied relatively slowly and quasi-statically. The protocol of loading is well-known and is widely used (e.g., Elgawady *et al*. 2006). This procedure begins as a series of three fully reversed load cycles to the same displacement magnitude and then displacement amplitude reduced by the same steps (the first decay cycle for one cycle each was 75 percent of the maximum displacement magnitude, second was 50 percent, and third was 25 percent). This process is repeated increasing the peak displacement value according to a prescribed history, until the end of the test. This pattern of horizontal loading makes possible to assess seismic parameters like strength deterioration, ductility, energy dissipation, pattern crack and failure mode which are vital for the conception of seismic response. The load protocol is presented in Fig. 5.

2.5 Instrumentation

Twelve linear variable displacement transducers (LVDTs) were installed to monitor deformations at different locations at horizontal, vertical, and diagonal directions, and to measure slip along the base and out-of-plane deformations. The horizontal displacement of the specimens relative to the concrete footing was measured by LVDTs 3 and 5. These displacements did not indicate any potential sliding mechanism for the specimens relative to the concrete footing. Fig. 6 shows the arrangement of the LVDTs. Several strain gauges were also placed on the external surface of the steel strips to measure the strains of the steel strips. Vertical and horizontal loads were measured using two load cells. The data were recorded digitally by a 30-channel data logger.

3. Experimental results

Table 3 Summary of the experimental results

Specimen	Crack pattern	Failure mode	Max. strength (kN)
URMW-1	LC/HC/DC	S	40.5
URMW-2	SC/DC	DT	21.2
EMW11SR-3	SC/VC/HC/DC	DT/TC/LBS	113.5
EMW21SSR-4	SC/HC/DC	DT/TC/LBS/FS	87.6

Note: DT=diagonal tension; S=sliding; TC=toe-crushing; LBS=local buckling of the steel strip; FS=fracture of the steel strip; LC=local cracking; SC=Spread cracking; DC= diagonal cracking; VC=vertical cracking; and HC= horizontal cracking.

In this section, the experimental results of the URM and retrofitted specimens are described in terms of crack pattern, failure modes and qualitative analysis of the load displacement hysteresis curves. A summary of the experimental results is presented in Table 3.

3.1 Reference specimens of URMW-1 and URMW-2

A summary of results of the reference specimens which had been previously tested is presented in Table 3 (Darbhanzi *et al*. 2014). The retrofitted specimens are described in the following sections.

3.2 Specimen EMW11SR-3

This specimen is similar to the reference specimen URMW-1. Retrofit was applied by adding one vertical steel strip in the middle of the wall and four diagonal steel strips on one wall face. In addition, the strips were fixed to foundation, as shown in Fig. 1. Horizontal cracks appeared at a displacement of 7.5 mm (Fig. 7(a)). By increasing lateral displacement, more diagonal, horizontal and vertical cracks appeared. At a lateral displacement of 10 mm, the first vertical crack (300 mm length) forms at the top, eastern edge, of the specimen (Fig. 7(b)) and this crack extends further at a displacement of 12.5 mm. At the end of test, this vertical crack widens to reach a width of 10 mm (Fig. 7(c)). Additional vertical cracks occur at the western edge of the specimen at a displacement of 15 mm. Local buckling of the diagonal steel strip also occurred at a displacement of 10 mm at the bottom end of the strips (Fig. 7(d)) and separation of the steel plates from the specimen at the end of test (Figs. 7(e) and 7(f)). The test was terminated at a displacement of 17.5 mm, and the observed damage indicate a combination of vertical and diagonal tension cracks, local buckling of steel strips and toe-crushing modes of failures, see Fig. 7. The hysteresis loops of Specimen EMW11SR-3 show relatively good energy dissipation capacity and a symmetrical response in both positive and negative directions, as shown in Fig.8. The maximum lateral strength was 113.5 kN at a displacement of 10mm.

3.3 Specimen EMW21SSR-4

This specimen is identical to the specimen URMW-2, but two diagonal and two vertical steel strips were added to one side of the wall. The steel strips were fixed to

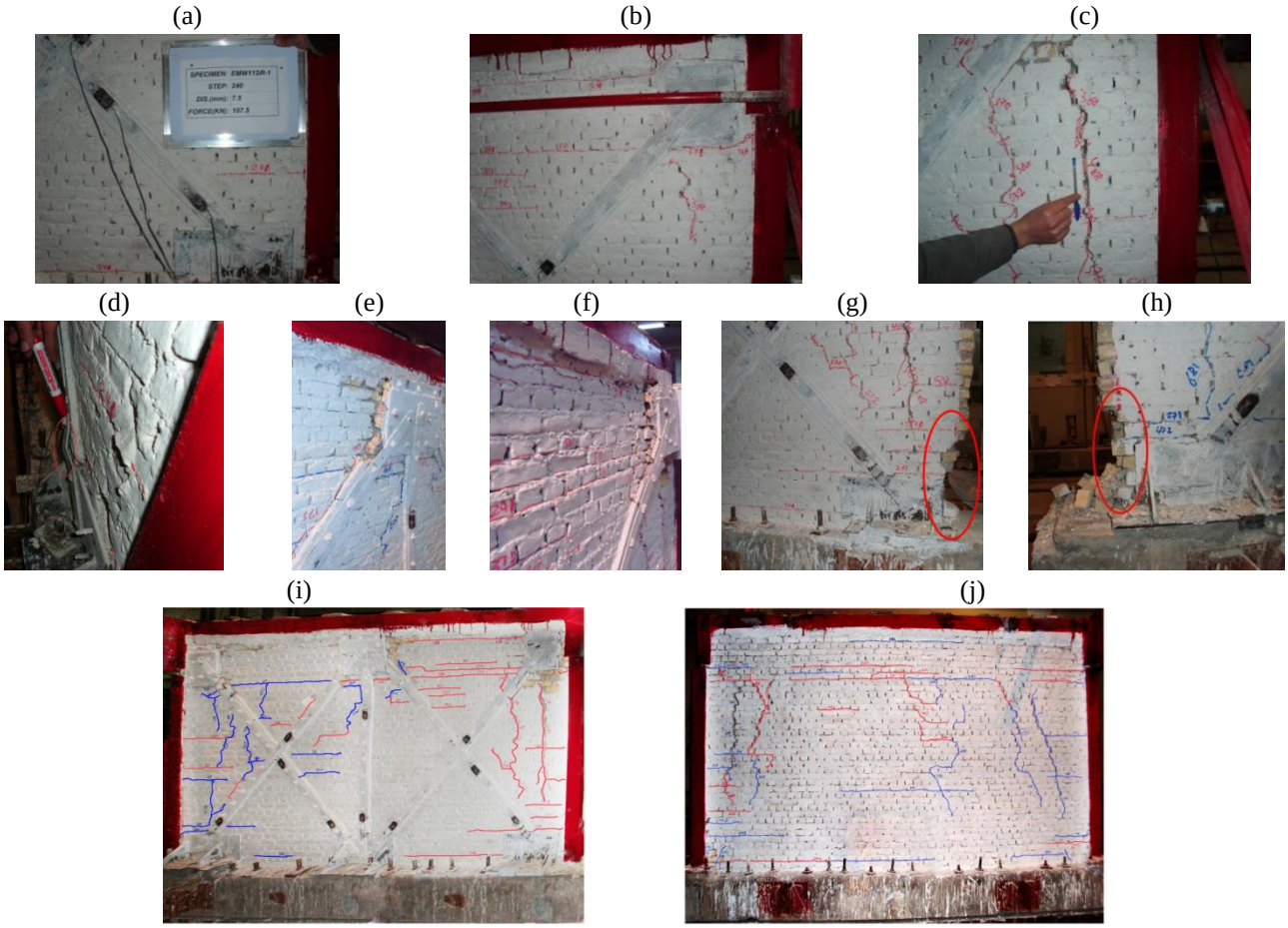

Fig. 7 Damage and crack patterns of Specimen EMW11SR-3 (a) Horizontal crack, (b) Vertical crack, (c) Width of vertical crack, (d) local buckling of steel strip, (e) and (f) separation of the steel plates from the specimen, (g) and (h) toe crushing, (i)Retrofitted surface end of test and (j) Unretrofitted surface end of test

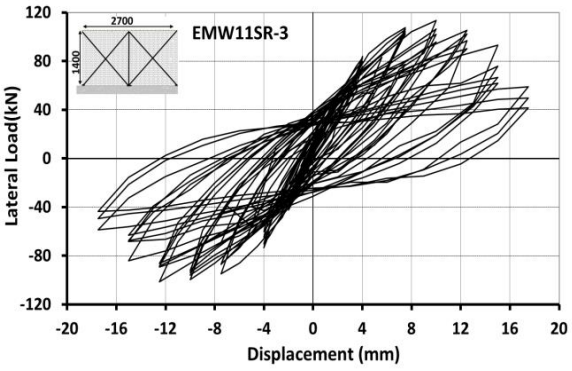

Fig. 8 Hysteresis curves of Specimen EMW11SR-3

foundation and shotcrete layers were added to top of both sides of Specimen EMW21SSR-4, as shown in Figs. 1 and 3. The first cracks appeared at a displacement of 3.5 mm (Fig. 9(a)). By increasing lateral displacement, more diagonal and horizontal cracks appeared. At a lateral displacement of 4 mm, the first diagonal crack formed at the top east corner of the specimen and this crack propagated towards the lower west corner at a displacement of 12 mm. At a lateral displacement of 14 mm, this diagonal crack widens to reach a width of 8 mm (Fig. 9(b)). The local buckling of the diagonal steel strip occurred at a displacement of 14 mm at the bottom end (Fig. 9(c)). The test was terminated at a displacement of 18 mm because of the fracture of the diagonal steel strip, see Fig. 9(d). The observed damage indicated a combination of diagonal tension, local buckling and rupture of steel strips, and toe-crushing modes of failures, see Fig. 9. The shape of hysteresis loops exhibits little pinching effect, as shown in Fig.10. At a lateral displacement of 14 mm, the maximum lateral strength recorded as 87.6 kN.

4. Comparison of retrofitted specimens with reference specimens

In this section, a comparison between the reference specimens and the retrofitted ones is presented. First, the experimental envelope curves of all specimens are analysed using a bilinear force-displacement relationship. Second, a comparison is made of lateral strength, lateral stiffness, failure mode, energy dissipation and ductility of all specimens.

4.1 Bilinear idealization

The bilinear idealization of the experimental envelope curves represents a basis for evaluation of the seismic

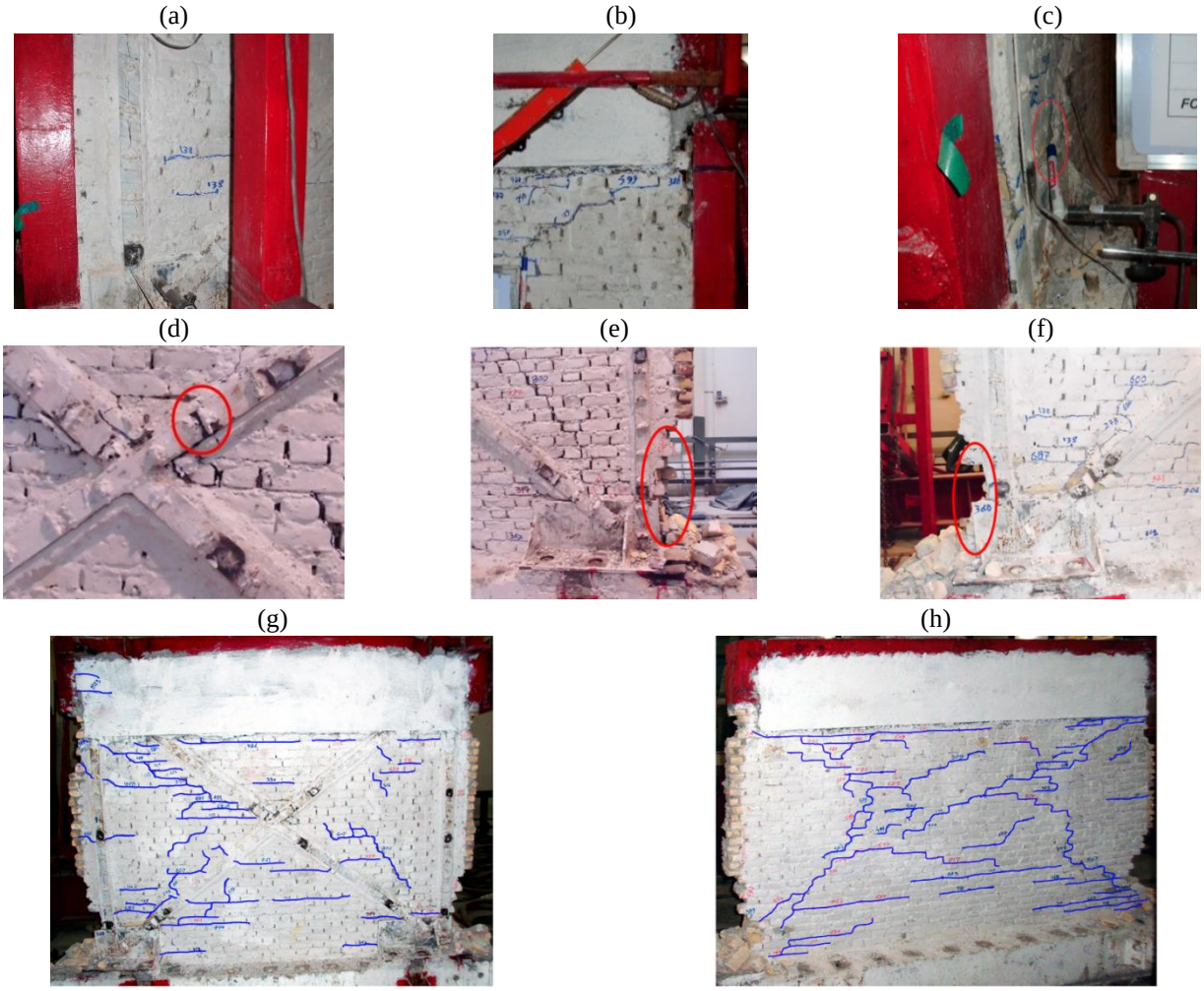

Fig. 9 Damage and crack patterns of Specimen EMW21SSR-4. (a) Horizontal crack, (b) Width of vertical crack, (c) loca buckling of steel strip, (d) fracture of steel strip, (e) and (f) toe crushing, (g)Retrofitted surface end of test and (h) Unretrofitte surface end of test

performance. According to the idealized curves, different characteristics such as ultimate strength, effective stiffness, and displacement ductility of all specimens are calculated.

This idealization method has been used by different references such as Paulay and Priestley (1992), Tomazevic *et al.* (2004), Lourenco *et al.* (2010), Sadek and Lissel (2013). The experimental results of all specimens are treated using the criteria stated in the following section (Lourenco *et al.* 2010, Sadek and Lissel 2013). The effective stiffness, K_e, is given by

$$K_e = \frac{H_{cr}}{d_{cr}} \tag{1}$$

where H_{cr} and d_{cr} are lateral load and lateral displacement at the first crack, respectively. The ultimate idealized strength, H_u, is defined as

$$H_u = K_e\left[d_{\max} - \sqrt{d_{\max}^2 - \frac{2A_{env}}{K_e}}\right] \tag{2}$$

where $d_{\max}$ and A_{env} are maximum displacement and area under the experimental envelope of the specimen, respectively. The ductility factor, μ, is calculated by

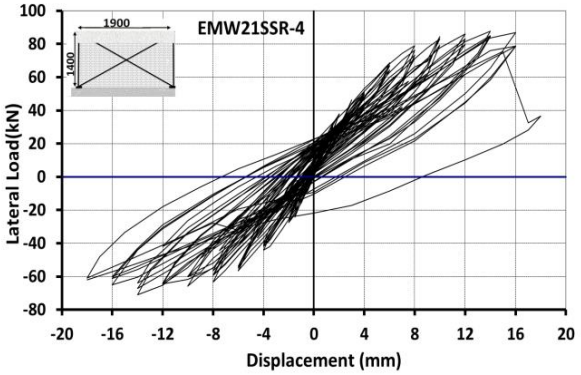

Fig. 10 Hysteresis curves of Specimen EMW21SSR-4

$$\mu = \frac{d_u}{d_e} \tag{3}$$

where d_u and d_e are ultimate idealized displacement and idealized effective displacement (yielding displacement) of the specimen, respectively.

Fig. 11 presents a typical idealized bilinear curve obtained from the hysteretic envelope of Specimen

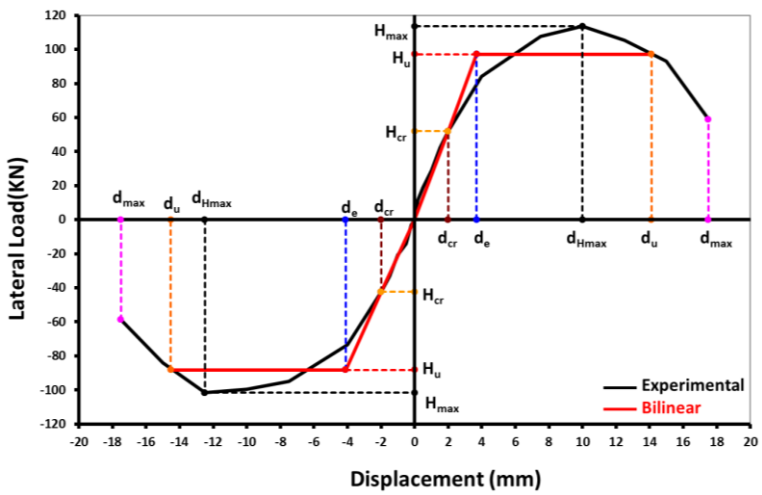

Fig. 11 Experimental cyclic envelope and the bilinear idealized curves of Specimen EMW11SR-3

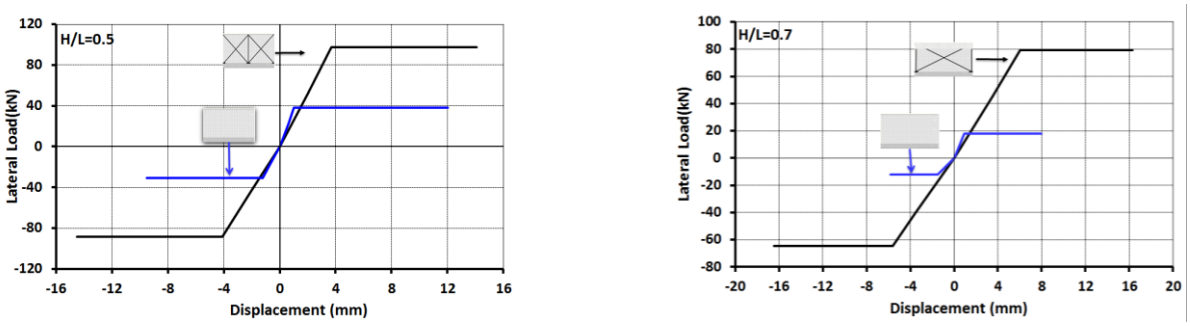

Fig. 12 Comparison of idealized curves of specimens with aspect ratio of 0.5 and 0.7

Table 4 Characteristic parameters of the hysteretic envelops and bilinear curves

Specimen	Aspect ratio	Bilinear	H_{cr} (kN)	d_{cr} (mm)	K_e (kN/mm)	H_u (kN)	d_e (mm)	H_{max} (kN)	H_u/H_{max}	d_{Hmax} (mm)	d_u (mm)	d_{max} (mm)	μ	Energy Dissipations (kN.mm)
URMW-1	0.5	Positive	23.1	0.63	36.67	38.09	1.04	40.5	0.94	10.00	12.03	15.0	11.6	8152.5
		Negative	16.0	0.63	25.40	30.93	1.22	35.0	0.88	7.50	9.50	15.0	7.8	4067.0
		average	19.6	0.63	31.04	34.51	1.13	37.8	0.91	8.75	10.77	15.0	9.7	6109.8
EMW11SR-3	0.5	Positive	51.9	2.00	25.95	97.14	3.74	113.5	0.86	10.00	14.11	17.5	3.8	4944.3
		Negative	42.4	2.00	21.20	88.19	4.16	101.6	0.87	12.50	14.52	17.5	3.5	9480.1
		average	47.2	2.00	23.58	92.67	3.95	107.6	0.86	11.25	14.32	17.5	3.7	7212.2
(EMW11SR-2/URMW-1))%			241	317	76	269	350	285	-	129	133	117	38	118.0
URMW-2	0.7	Positive	17.9	0.90	19.89	17.90	0.90	21.2	0.84	3.00	7.96	14.0	8.8	213.5
		Negative	7.3	0.90	8.11	12.23	1.51	15.4	0.79	4.20	5.81	14.0	3.9	451.9
		average	12.6	0.90	14.00	15.07	1.21	18.3	0.82	3.60	6.89	14.0	6.4	332.7
EMW21SSR-4	0.7	Positive	45.9	3.50	13.11	79.35	6.05	87.6	0.91	14.00	16.30	18.0	2.7	5084.8
		Negative	40.5	3.50	11.57	64.46	5.56	71.7	0.91	14.00	16.44	18.0	3	5084.8
		average	43.2	3.50	12.34	71.91	5.8	79.7	0.90	14.00	16.37	18.0	2.9	5084.8
(EMW21SSR-4/URMW-2)%			343	389	88	477	408	435	-	389	238	129	45	1528.3

EMW11SR-3. The idealized curves of all specimens are shown in Fig. 12. The characteristic parameters of the experimental envelopes as well as those of the idealized curves are summarized in Table 4.

4.2 Strength

The envelope and hysteresis curves of all specimens are plotted in Figs. 13 and 14, respectively. As can be observed from Table 4 and Figs. 13 and 14, the maximum lateral strengths of the specimens EMW11SR-3 and EMW21SSR-4 are 185% and 335%, higher than those of the specimens URMW-1 and URMW-2, respectively. On the other hand, based on the bilinear idealization curve and Table 4, for specimens EMW21SSR-4 and URMW-1, the value of 0.9 was calculated for the ratio between ultimate idealized

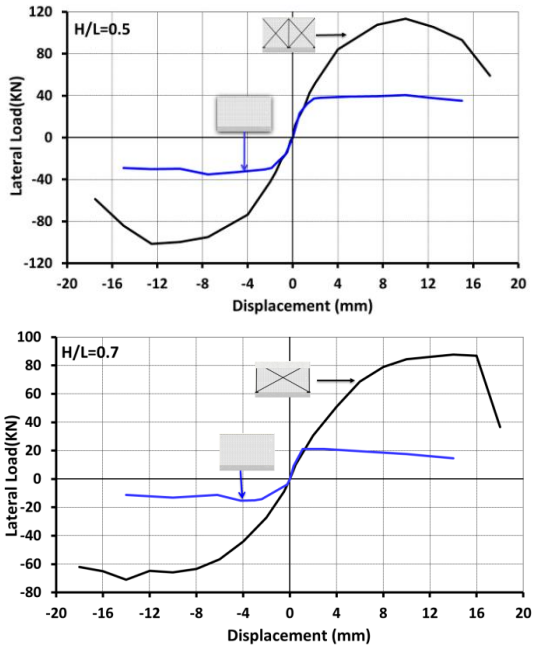

Fig. 13 Comparison of envelope curves of specimens with aspect ratios of 0.5 and 0.7

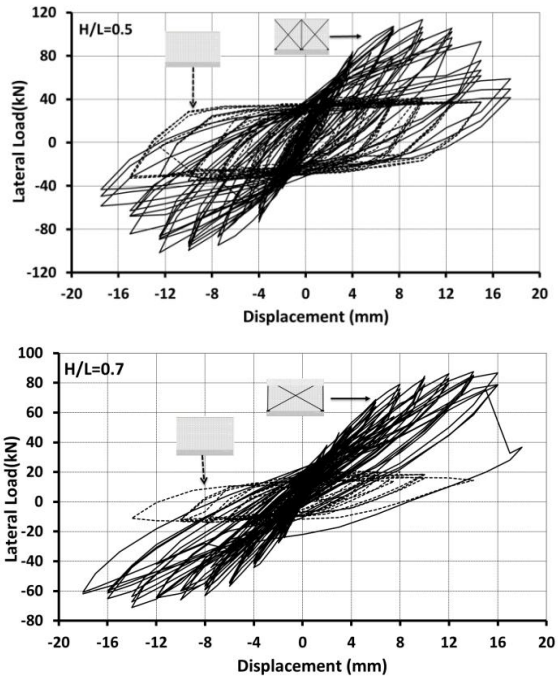

Fig. 14 Comparison of hysteresis curves of specimens with aspect ratios of 0.5 and 0.7

strength (H_u) and experimental maximum strength (H_{max}), which is equal to the value pointed out by Tomazevic *et al*. (1996) and Marcari *et al*. (2007). The value of ratio H_u/H_{max}=0.82 was calculated for specimen URMW-2, which show very brittle behavior according to studied performed by Lourenco *et al*. (2010). Specimen EMW11SR-1 failed in shear and the value of ratio H_u/H_{max}=0.86 was obtained.

4.3 Failur modes

Different failure modes occurred during the tests. The observed failure modes of the reference specimens URMW-1 and URMW-2 were shear slip and diagonal tension, respectively. The retrofitting technique changed the failure modes. The failure modes of retrofitted specimens were diagonal tension, toe-crushing and local buckling of the steel strips.

4.4 Ductility

The values of ductility of different specimens are presented in Table 4. As can be observed, all the reference specimens have shown higher ductility compared with the retrofitted ones. The results are comparable to those reported by Churilov *et al*. (2013), Mahmood *et al*. (2011), Magenes *et al*. (2008), Vasconcelos *et al*. (2005) and based on the definition of ductility according to Fig. 11. The relatively large values of ductility may be attributed to both definition of yield point and initiation of damage and crack at relatively early stages for the reference specimens. That is, the idealized curves of the reference specimens have dictated a small yield displacement which has resulted in a relatively large value for ductility. On the other hand, the behavior of the specimen URMW-1 was sliding mode. According to studies conducted by Magenes *at el*. (1997), the specimen has a large deformation capacity.

4.5 Stiffness

Effective stiffness is explained in Fig. 11, where the hysteretic envelope curve of an actual wall, idealized by a bilinear curve. The values of effective stiffness of all specimens are presented in Table 4. On the basis of Table 4, the effective stiffness of the specimens URMW-1 and URMW-2 are 24% and 12% larger than the specimens EMW11SR-3 and EMW21SSR-4, respectively. This subject indicated by the lower slope of the idealized curves of retrofitted specimens (Fig. 12). This is not a great improvement and indicates that the retrofitting technique has relatively little influence on the effective stiffness. To the authors' view, the relatively large variation in the results may be explained by relatively large uncertainties in properties of masonry walls and relatively small contribution of the steel strips to overall stiffness of the wall.

4.6 Energy dissipation

Values of cumulative hysteresis energy dissipation of different specimens at the maximum strength are presented in Table 4. This is an important factor in the evaluation of the seismic performance. On the basis of Table 4, the energy dissipation of the specimens EMW11SR-3 and EMW21SSR-4 are 18% and 1500% higher than those of the specimens URMW-1 and URMW-2, respectively. The high energy dissipation capacity of the specimen URMW-1 was due to the failure of the specimen in a sliding mode, as expressed in research by Magenes *at el*. (1997).

5. Conclusions

This paper presents results of an experimental research on seismic retrofitting of URM walls. The retrofitting technique comprises addition of both vertical and diagonal steel strips on one side of the walls. In total, four specimens have been tested: two specimens with steel strips on one side where the strips are fixed to foundation, and two specimens without strips as reference specimens. The specimens were subjected to quasi-static cyclic lateral load in combination with constant vertical load. According to the tests, addition of vertical and diagonal strips to URM walls causes:

- increase of maximum strengths by more than 185% and 335% respectively, for specimen with aspect ratio of 0.5 and 0.7,
- increase of yield strengths by more than 140% and 240% respectively, for specimen with aspect ratio of 0.5 and 0.7,
- increase of displacement at yield by more than 200%,
- increase of displacement at maximum by about 20%,
- little reduction of effective stiffness by more than 10%,
- increase of energy dissipation at maximum strengths by more than 15% and 14 time respectively, for specimen with aspect ratio of 0.5 and 0.7,
- transform of failure mode from shear slip (URMW-1) and diagonal tension (URMW-2) into a combination of diagonal tension and toe-crushing for all retrofitted specimens.

As a general conclusion, this study shows that seismic capacity of the specimens increases significantly with the addition of diagonal and vertical steel strips to one side of URM walls. This method is simple and bears relatively low costs.

References

Abdul Karim, A.R., M.Sa'don, N. and Ingham, J.M. (2016), "Structural dynamic response of an unreinforced masonry house using non-destructive forced vibration", *J. Earthq. Eng.*, **20**, 1-11.

Ahmad, Z., Shahzada, K., Gencturk, B., Naeem Khan, A., Rehan, R., Fahad, M., Ashraf, M. and Ali, Z. (2015), "Seismic capacity assessment of unreinforced concrete block masonry buildings in Pakistan before and after retrofitting", *J. Earthq. Eng.*, **19**, 357-382.

ASTM C1314 (2002), Standard Test Method for Compressive Strength of Masonry Prisms, American Society for Testing of Materials (ASTM), USA.

ASTM C1531 (2002), Standard Test Methods for in Situ Measurement of Masonry Mortar Joint Shear Strength index, American Society for Testing of Materials (ASTM), USA.

ASTM C67 (2002), Standard Test Method for Sampling and Testing Brick and Structural Clay Tile, American Society for Testing of Materials (ASTM), USA.

ASTM E8/E8M-09 (2009), Standard Test Methods for Tension Testing of Metallic Materials, American Society for Testing of Materials (ASTM), USA.

Benedetti, A., Landi, L. and Merenda, D.G. (2014), "Displacement-based design of an energy dissipating system for seismic upgrading of existing masonry structures", *J. Earthq. Eng.*, **18**, 477-501.

Churilov, S. and Dumova-Jovanoska, E. (2013), "In-plane shear behaviour of unreinforced and jacketed brick masonry walls", *Soil Dyn. Earthq. Eng.*, **50**, 85-105.

Darbhanzi, A., Marefat, M.S. and Khanmohammadi, M. (2014), "Investigation of in-plane seismic retrofit of unreinforced masonry walls by means of vertical steel strips", *Constr. Build. Mater.*, **52**, 122-129.

ELGawady, M.A., Lestuzzi, P. and Badoux, M. (2006), "Shear strength of URM walls retrofitted using FRP", *Eng. Struct.*, **28**, 1658-1670.

Farooq, S.H., Ilyas, M. and Amir, S. (2012), "Response of masonry walls strengthened with CFRP and steel strips", *Arab J. Sci. Eng.*, **37**, 545-559.

Lourenco, P.B., Vasconcelos, G., Medeiros, P. and Gouveia, J. (2010), "Vertically perforated clay brick masonry for loadbearing and non-loadbearing masonry walls", *Constr. Build. Mater.*, **24**, 2317-2330.

Magenes, G. and Calvi, GM. (1997), "In-plane seismic response of brick masonry walls", *Earthq. Eng. Struct. Dyn.*, **26**, 1091-1112.

Magenes, G., Morandi, P. and Penna A. (2008), "experimental in-plane cyclic response of masonry walls with clay units'', *Proceedings of the 14th World Conference on Earthquake Engineering*, Beijing, China.

Mahjoob Farshchi, D., Motavalli, M., Schumacher, A. and Marefat, M.S. (2009), "Numerical modeling of in-plane behaviour of URM walls and an investigation into the aspect ratio, vertical and horizontal post-tensioning and head joint as a parametric study", *Arch. Civil Mech. Eng.*, **9**(1), 5-27.

Mahmood, H. and Ingham, J.M. (2011), "Diagonal compression testing of FRP-retrofitted unreinforced clay brick masonry wallettes", *J. Compos. Constr.*, ASCE, **15**(5), 810-820.

Marcari, G., Manfredi, G., Prota, A. and Pecce, M. (2007), "In-plane shear performance of masonry panels strengthened with FRP'', *Compos. Part B*, **38**, 887-901.

Medeiros, P., Vasconcelos, G., Lourenco, P.B. and Gouveia, J. (2013), "Numerical modelling of non-confined and confined masonry walls", *Constr. Build. Mater.*, **41**, 968-976.

Paulay, T. and Priestley, M.J.N. (1992), *Seismic Design Of Reinforced Concrete And Masonry Buildings*, Wiley-Interscience, New York.

Popa, V., Pascu, R., Papurcu, A. and Albota, E. (2016), "Retrofitting of squat masonry walls by FRP grids bonded by cement-based mortar", *Earthq. Struct.*, **10**(1), 125-139.

Porter, M.L. (1987), "Sequential phased displacement (SPD) procedure for TCCMAR testing", Report of the Third Meeting of the US-Japan Joint Technical Committee on Masonry Research, Tomaru, Japan.

Preciado, A., Ramirez-Gaytan, A., Salido-Ruiz, A.R., Caro-Becerra, L.J. and Lujan-Godinez, R. (2015), "Earthquake risk assessment methods of unreinforced masonry structures: Hazard and vulnerability", *Earthq. Struct.*, **9**(4), 719-733.

Remki, M., Kehila, F., Bechtoula, H. and Bourzam, A. (2016), "Seismic vulnerability assessment of composite reinforced concrete-masonry building", *Earthq. Struct.*, **11**(2), 371-386.

Sadek, H. and Lissel, S. (2013), "Seismic performance of masonry walls with GFRP and geogrid bed joint reinforcement", *Constr. Build. Mater.*, **41**, 977-989.

Taghdi, M., Bruneau, M. and Saatcioglu, M. (2000), "Seismic retrofitting of low-rise masonry and concrete walls using steel strips", *J. Struct. Eng.*, ASCE, **126**(9), 1017-1025.

Tena-Colunga, A., Juárez-Á ngeles, A., Víctor, H. and Salinas-Vallejo, V.H. (2009), "Cyclic behavior of combined and confined masonry walls", *Eng. Struct.*, **31**, 240-259.

Tomazevic, M. (1996), "Recent advances in earthquake-resistant design of masonry buildings", *Proceedings of the 11th World Conference on Earthquake Engineering*, Acapulco, Paper No. 2012.

Tomazevic, M., Bosiljkov, V. and Weiss, P. (2004) "Structural behavior factor for masonry structures", *Proceedings of the 13th Conference on Earthquake Engineering*, Vancouver, Canada.

Vasconcelos, G. and Lourenco, P.B. (2005), "Evaluation of the in-plane seismic performance of stone masonry walls'', *Proceedings of the 5th International Conference (AMCM 2005)*, Gliwice-Ustron, Poland.

Wang, Q., Chai, Z. and Wang, L. (2014), "Seismic capacity of brick masonry walls externally bonded GFRP under in-plane loading", *Struct. Eng. Mech.*, **51**(3), 413-431.

Zuccarello, F.A., Milani, G., Olivito, R.S. and Tralli, A. (2009), "A numerical and experimental analysis of unbonded brickwork panels laterally loaded", *Constr. Build. Mater.*, **23**, 2093-2106.

AT